World Electric Vehicle Journal

MDPI

Article

On the Development and Experimental Validation of a Novel and Intuitive Interior Permanent Magnet Synchronous Motor Controller for Electric Vehicle Application

Muhammad Nur Yuniarto [1,*], Indra Sidharta [1], Yohanes Yohanes [1] and Yoga Uta Nugraha [2]

[1] Department of Mechanical Engineering, Institut Teknologi Sepuluh Nopember, Surabaya 60111, Indonesia; sidarta@me.its.ac.id (I.S.); yunus@me.its.ac.id (Y.Y.)
[2] Faculty of Advanced Technology and Multidicipline, Universitas Airlangga, Surabaya 60115, Indonesia; yoga.uta.n@ftmm.unair.ac.id
* Correspondence: mnur@me.its.ac.id; Tel.: +62-8133-127-3856

Abstract: This paper discusses the process of developing a novel and robust algorithm for an interior permanent magnet synchronous motor controller. This is necessary for the simplification of the setting of control parameters and maintaining the proper operation of the motor. A 3D torque lookup table was used in which two inputs were considered, i.e., accelerator movements and the motor rotational speed. These two inputs allowed the lookup table to generate a specified torque at any motor rotation, which was then fed-forward to the field-oriented control and space vector pulse width modulation algorithm. Modeling, simulation, and experimental tests were performed to design and validate the proposed controller. The experimental validation shows that the proposed controller worked as intended. This was indicated by its ability to control the motor to obtain a 7% higher torque output than in the simulation in the constant torque region. In the field-weakening region, the controller could make the motor reach a maximum speed of 5500 RPM. There was only an 8% difference compared to the simulation (6500 RPM). In terms of maximum power generated, the controller was able to match the simulation output with only a 5% difference.

Keywords: three-dimensional lookup table; electric vehicle; field-oriented control; field weakening; novel and intuitive controller; lookup table; space vector pulse width modulation; PI controller; interior permanent magnet synchronous motor

check for updates

Citation: Yuniarto, M.N.; Sidharta, I.; Yohanes, Y.; Nugraha, Y.U. On the Development and Experimental Validation of a Novel and Intuitive Interior Permanent Magnet Synchronous Motor Controller for Electric Vehicle Application. *World Electr. Veh. J.* **2022**, *13*, 107. https://doi.org/10.3390/wevj13060107

Academic Editors: Syed Sabir Hussain Bukhari, Jorge Rodas and Jesús Doval-Gandoy

Received: 20 May 2022
Accepted: 16 June 2022
Published: 20 June 2022

Publisher's Note: MDPI stays neutral with regard to jurisdictional claims in published maps and institutional affiliations.

Copyright: © 2022 by the authors. Licensee MDPI, Basel, Switzerland. This article is an open access article distributed under the terms and conditions of the Creative Commons Attribution (CC BY) license (https://creativecommons.org/licenses/by/4.0/).

1. Introduction

The permanent magnet synchronous motor (PMSM) and interior permanent magnet synchronous motor (IPMSM) are proven by their nature to be promising options for use in an electric vehicle traction motor, but some challenges need to be addressed in terms of their implementation. Some of these have been previously reported in several studies, such as the voltage and current limitation constraints identified in work by [1]. A novel algorithm known as the discrete-time field-oriented control was implemented in the IPMSM controller and observed to have produced optimal torque dynamics over full speed operation range. The authors of [2] also identified torque loss control in PMSM due to heavy-load or high-speed operating conditions and proposed a load-angle-feedback direct torque control solution. The experiment, validation, and analysis of their research showed that the proposed modifications to the current direct torque control were able to extend the motor operating conditions, including the wider load capacity and speed operation range. An improvement of direct torque control to deal with torque loss was proposed by [3]. They used the so-called firefly algorithm combined with a fractional order PID controller. Moreover, Ref. [4] confirmed that a PMSM experienced instability issues during overloading and its overload capabilities were heavily dependent on the speed. The investigation was discovered to focus on implementing the IPMSM as a servo drive

with the proposal of a modified direct torque control space vector machine to solve the instability issues.

This research focused on developing an alternative IPMSM controller algorithm in electric vehicles. It is based on an engine controller unit (ECU) philosophy. The ECU has been reported to usually deal with nonlinearities due to variations of the operating point when applied in electric vehicles or automotive fields [5]. The operating point is typically a combination of the function of the engine speed n and the engine torque T, which are dynamically or rapidly changing due to the load and driving behavior. Therefore, there is the need to design a robust controller to cope with the problem. Previous studies agreed that there are current drawbacks in implementing the IPMSM controller for electric vehicles due to its dynamic nature, which is reflected in the need for higher flexibility with the ever-changing torque and RPM requirements. This is a nonlinear phenomenon considered unsolvable using most conventional control algorithm methods that are assumed to be based on linear phenomenon [6]. Therefore, this study proposed an alternative framework incorporating the torque versus rotational speed and field-weakening lookup tables into the FOC algorithm. The torque lookup table, however, consists of two inputs, including the accelerator degree of movement and the rotational speed of the IPMSM. The interaction between them was designed to represent the load to be handled at any point of the operating speed. The introduction of the two inputs is more intuitive as it directly measures driver behaviors into the lookup table. Furthermore, it is more practical, as is the case with the engine controller unit (ECU) in conventional (internal combustion engine-driven) vehicles. Meanwhile, the field-weakening lookup table was used to control the motor beyond its base rotational speed. The IPMSM controller also needs to possess a real-time capability to handle such dynamic and ever-changing operation [7,8]. Several control algorithms have been proposed to deal with these situations and were categorized into feedback, feedforward, and a mixture of feedback and feedforward control algorithms [9,10]. These algorithms use current, voltage, and torque as input parameters based on IPMSM governing equations for the constant torque region in Equation (14) and the constant power/flux weakening region in Equation (15).

The authors of [11,12] used current errors in i_d and i_q as feedback signals in their method of improving PMSM control and applied the current errors in the hysteresis current regulator of the controller. Other works reporting on this development area were conducted by [13,14], using voltage as the feedback to improve the PMSM control algorithm. However, work carried out by [15,16] found that using current error and voltage error as feedback signals in the PMSM controller has a limitation: the inability to determine the optimal current operating point. This led to a proposal of another method to improve the PMSM controller performance using torque and motor speed as the signals for the feedforward control algorithm. The process involved setting a torque and field-weakening 3D lookup table based on the IPMSM performance determined through torque vs. speed and torque vs. efficiency curves. It is important to note that the 3D torque lookup table has the ability to examine two inputs, accelerator movements and IPMSM rotational speed, usually used in generating a specified torque and subsequently fed forward to the FOC-SVPM algorithm. Moreover, the 3D torque lookup table enables the users to input easily and intuitively the targeted torque for each operating point. In this case, the torque curve from the IPMSM modeling and simulation was used as the source for the targeted torque. It is also important to note that the torque versus rotational speed curve is the most important characteristic of an electric motor. However, the information contained in this curve is rarely used in developing controller algorithms, with most programmers observed to only focus on the maximum value required to limit the electric motor operating point.

The lookup table had been applied to control IPMSM as indicated in the previous studies [17]. They proposed to use the lookup table to improve the IPMSM performance in high-torque, low-speed applications around field weakening. The lookup table was based on the calculated value for both d-axis current using an offline method as well as the online calculation of q-axis current using the torque equation. The results still showed

the proposed methodology was unable to meet the desired target. This was observed to be due to the coupling phenomenon on the d- and q-axes as well as the variation of the motor parameters. Nevertheless, the lookup table was discovered to have the ability to improve the PMSM performance over a wider range of operations. The lookup table constructed from experimental data, such as the dynamometer test, is superior to that estimated from calculation as shown by [18]. They proposed torque output improvement based on constructing a lookup table-based controller by characterizing it to ensure it is applicable in a wide operation range, such as in an electric traction motor for an electric vehicle. Moreover, it focused on improving IPMSM controller performance, especially in the field-weakening area. This involved using lookup tables of motor rotation and the motor torque feedforward technique to derive torque command for the weakening field operation. The experimental results showed the technique's ability to maximize the output torque and improve torque stability in the flux weakening field.

The viability of implementing the lookup table in the PMSM controller has been reported by several researchers [19,20]. They were both employing the torque and rotational speed of the PMSM as the inputs of their controllers. They introduced a feedforward interpolation compensation error for different ranges of the PMSM operation. The authors of [19] focused on the performance evaluation of their proposed controller in the field-weakening region while [20] focused their research on the maximum power control region. Their lookup table contains a discrete torque map. An extensive set of torque data is required to explore the best performance of this method. However, some controllers have insufficient memory to contain all those data. Linear interpolation is commonly used to obtain an estimated torque based on limited data. However, the linear interpolation method does not match the nonlinear characteristic of PMSM. The authors of [20] added a compensation block to correct the linear interpolation using DC-link voltage feedforward and obtain precise output torque from the limited data. Later, Ref. [19] improved the compensation method using two feedforward compensators and a PI controller. This method is beneficial if we use a controller with limited memory. Both reported that their lookup table compensation could improve the performance of the conventional lookup table controller.

The electric motor performance curves were used in this research as the basis for the torque and field-weakening lookup table, as previously explained, to ensure the direct development of the controller. The curves also allow the users of the proposed controller to specify the targeted torque to match specific requirements intuitively. Moreover, they make the controller easily reprogrammable to work with any electric motor in the same class. These performance curves also contain information on the working envelope of electric motors and ensure the controller no longer needs its limiter values (as in the case of [19,20]) after they have been incorporated using the torque and field-weakening lookup tables. Furthermore, the lookup table aids the safe operation of the controller by integrating the maximum value of torque, current, and current ramping up in the system. This is mainly required when the motor is subjected to ever-increasing and changing loads. The novelty of the paper is in its simplified approach of integrating all electric motor parameters into one 3D lookup table to obtain maximum performance on each operating point (torque:RPM) of the motor in the whole range of its operation.

The paper is organized as follows: Section 2 discusses the methodology of the proposed work. It includes a mathematical model of the FOC algorithm for IPMSM controller and MATLAB or Simulink model to estimate the performance of the proposed IPMSM controller. Section 3 explains the experimental setup to validate the performance of the controller. Subsequently, Sections 4 and 5 discuss the experimental results and conclusions, respectively.

2. Methodology

2.1. Basic Mathematical Control Equations of the 3-Phase V-Shaped IPMSM

The permanent magnet synchronous motor (PMSM) investigated is the 3-phase interior mounted permanent magnet motor presented in Figure 1. It was developed by the authors of [21] in 2021 to be used in an electric utility vehicle.

Figure 1. Exploded view of the PMSM to be controlled by the proposed controller.

According to Figure 1, the PMSM has three phases and a V-shaped interior permanent magnet synchronous motor (IPMSM) with the specifications tabulated in Table 1.

Table 1. Specifications of the proposed interior permanent magnet synchronous machine (IPMSM).

Parameter	Value	Unit
Stator outer/inner diameters	180	mm
Rotor outer/inner diameters	108	mm
Tooth width	15.9	mm
Tooth depth	22	mm
Stack length	90	mm
Magnet type/thickness	N42H/5	mm
Magnet width	90	mm
Magnet angle	43	Deg (°)
Slots/poles (SP)	12/8	
Air-gap	1	mm
Rated power	20	kW
Rated speed	6000	RPM
Rated torque	82	Nm
Phase	3	Phase
Direct current (DC) link voltage	100	V
Peak current	550	A
RMS current	389	A
Inertia	0.007629	Kgm^2
Resistance	0.002405	Ohms
D-axis inductance	0.00002939	H
Q-axis inductance	0.00004914	H
D-axis reactance	0.0714	Ohms
Q-axis reactance	0.1194	Ohms
Flux linkage D (Q-axis current)	20.2085	mVs
Flux linkage Q (Q-axis current)	14.6478	mVs
Flux linkage D (on load)	10.8567	mVs
Flux linkage Q (on load)	15.6358	mVs
Phase (elec deg)	45	Deg (°)
Drive mode	Sine	
Winding connection	Star/Wye	
Magnetization	Radial	

The permanent magnets of the V-shaped PMSM are embedded into the rotor in the V-shaped configuration as presented in Figure 2, making it mechanically robust for high-speed applications. The figure shows the three-phase V-shaped IPMSM (8 poles) along with its direct (*d*-) and quadrature (*q*-) magnetic and its three-phase axis definition.

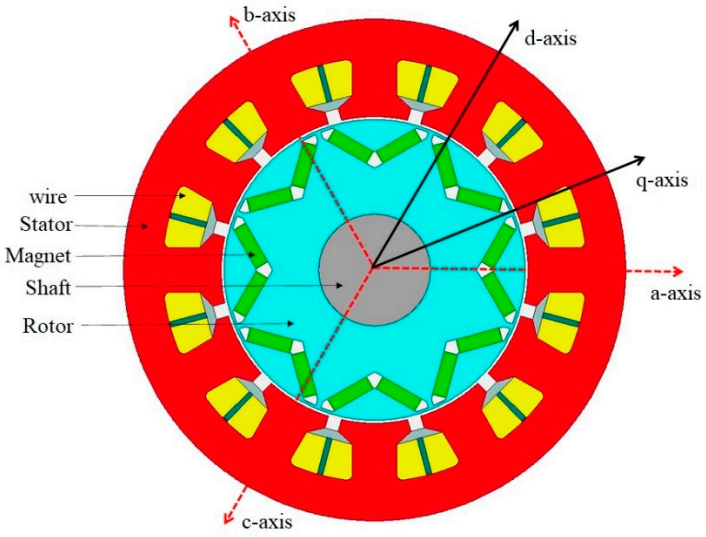

Figure 2. The three-phase V-shaped IPMSM with eight poles of magnets *d*- and *q*-axis definition.

It is possible to approach the mathematical model of the three-phase V-shape IPMSM as a generic radial magnetization of IPMSM, as suggested by [22]. This involves aligning the d-axis with the maximum reluctance axis. Moreover, the peak reluctance and peak magnet torque in the conventional PMSMs in this system were also phase-shifted by 45°. Therefore, the mathematical expressions were, therefore, defined by several works [23–27] to be written as follows.

$$\begin{bmatrix} \psi_q \\ \psi_d \end{bmatrix} = \begin{bmatrix} L_q & 0 \\ 0 & L_d \end{bmatrix} \begin{bmatrix} i_q \\ i_d \end{bmatrix} + \psi_m \begin{bmatrix} 0 \\ 1 \end{bmatrix} \tag{1}$$

$$\begin{bmatrix} v_q \\ v_d \end{bmatrix} = r_s \begin{bmatrix} i_q \\ i_d \end{bmatrix} + \frac{d}{dt} \begin{bmatrix} \psi_q \\ \psi_d \end{bmatrix} + \omega_r \begin{bmatrix} 0 & 1 \\ -1 & 0 \end{bmatrix} \begin{bmatrix} \psi_q \\ \psi_d \end{bmatrix} \tag{2}$$

$$T_e = \frac{3}{2} P \left[\psi_m i_q + \left(L_d - L_q \right) i_q i_d \right] \tag{3}$$

This equation shows that the i_d current must be a negative value to achieve positive reluctance torque since the direct inductance (L_d) is larger than the quadrature inductance (L_q). The parameters used in these equations include ψ_m which is the magnetic flux linkage, $\psi_q = L_q i_q, \quad \psi_d = \psi_m + L_d i_d$ are the *q*- and *d*-axis inductances, respectively, v_q, v_d and i_q, i_d are the *q* and *d* reference frame voltages and current while r_s is the stator resistance, ω_r is the angular speed of the rotor (electrical angular speed), and P is the IPMSM number of magnet poles.

Newton's second law was later applied to Equation (3) to obtain the equation of motion for the generic IPMSM as follows:

$$T_e - T_L = J \frac{d\omega_m}{dt} \tag{4}$$

where T_L is the load torque, J is the IPMSM rotor inertia, and ω_m is the mechanical angular speed of the IPMSM rotor which is equal to $\frac{\omega_r}{P}$. The representation of i_q and i_d as a vector in *d;q* rotating current reference frame can be presented in Figure 3. In the figure, θ is defined as the rotor position angle or in this case as the current phase angle between i_d and i_q in its *d*-axis reference.

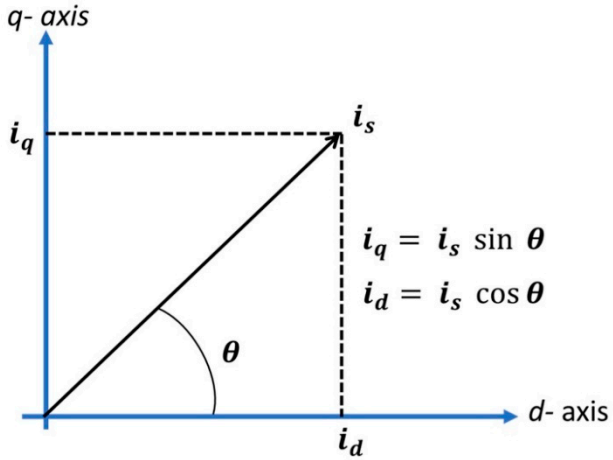

Figure 3. Vector representation of i_q and i_d in rotating current reference frame (d;q).

The substitution of $i_q = i_s \sin\theta$ and $i_d = i_s \cos\theta$ in Equation (3) generated the torque for the IPMSM with respect to its rotating reference frame d;q as follows.

$$T_e = \frac{3}{2}P\left[\psi_m i_s \sin\theta + \frac{1}{2}(L_d - L_q) i_s^2 \sin 2\theta\right] \tag{5}$$

where i_s is the total current vector (current commanded in IPMSM controller). Figure 3 shows that

$$i_q{}^2 + i_d{}^2 = i_s{}^2 \tag{6}$$

and its voltage in q and d rotating reference frame can be derived as:

$$v_q{}^2 + v_d{}^2 = v_s{}^2 \tag{7}$$

From the practical perspective or real-life application, i_s and v_s have their maximum values, which are denoted as $i_{s_{Max}}$ and $v_{s_{Max}}$ respectively in this case. The substitution of these values in Equations (6) and (7) leads to the following equations.

$$i_q{}^2 + i_d{}^2 \leq i_{s_{Max}}{}^2 \tag{8}$$

$$v_q{}^2 + v_d{}^2 \leq v_{s_{Max}}{}^2 \tag{9}$$

Therefore, Equations (8) and (9) are the current and voltage limit of the IPMSM under investigation. The substitution of Equations (1) and (2) in Equation (9) makes the IPMSM voltage limit become,

$$\left(r_s i_q + \omega_r (L_d i_d + \psi_m)\right)^2 + \left(r_s i_d - \omega_r L_q i_q\right)^2 \leq v_{s_{Max}}{}^2 \tag{10}$$

One of the advantages of the IPMSM is its suitability for electric vehicle application due to its mechanically robust rotor structure with a low effective air gap considered to be effective in flux weakening operation. Therefore, it makes the IPMSM applicable in the higher RPM region, not only in the constant torque region. Therefore, the typical torque-rotational characteristics of the IPMSM are presented in the following Figure 4.

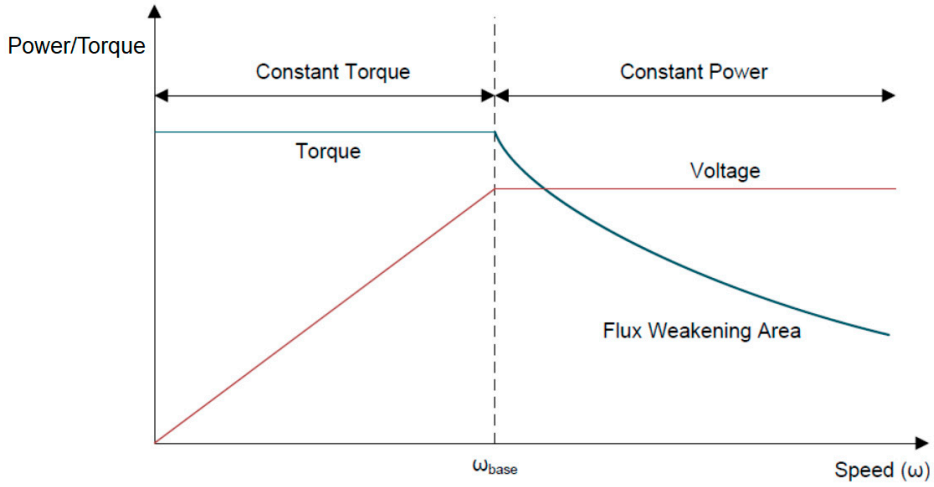

Figure 4. Typical torque rotational-speed characteristics of the IPMSM.

Figure 4 shows the two regions of the IPMSM operation range. The first is the constant torque region which allows it to generate constant torque up to the period the maximum value of any rotational speed is less than its base or rated speed. The second is the flux weakening region when the rotational speed is higher than the rated speed, thereby granting the IPMSM the ability to generate constant power with reduced torque until its no-load rotational speed. Therefore, the mathematical models and equations for these regions were derived in the next subsection.

2.2. Proposed Control Algorithm for the IPMSM

As explained in the previous section, there is a need to develop a control algorithm to improve the PMSM controller performance. It can be realized by employing a mixed feedforward and feedback algorithm, as depicted in Figure 5. As shown in Figure 5, the proposed control algorithm uses a lookup table derived from current, torque and efficiency maps obtained from an IPMSM motor design modelling and simulation. The proposed control algorithm uses the values from the current and efficiency maps of the motor as the feedforward inputs for the FOC controller. By doing so, it is expected the motor can be operated at maximum capacity and efficiency. Moreover, the feedforward mechanism can also make the motor change its output, based on the changing conditions in real-time.

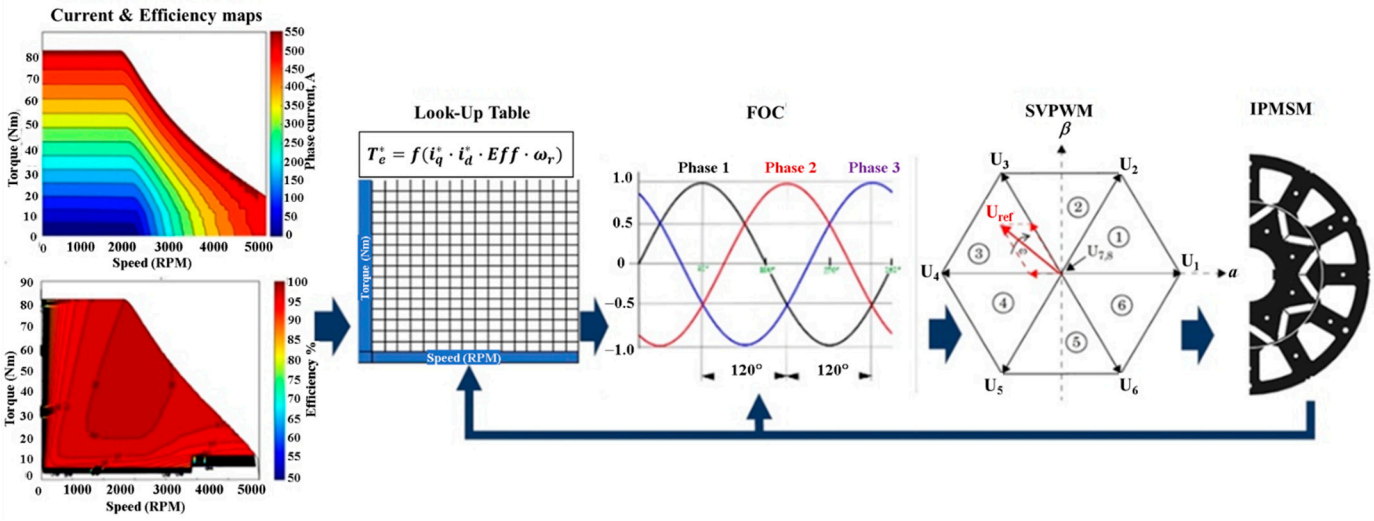

Figure 5. The proposed framework to control the IPMSM.

The model was subsequently integrated into a current field-oriented control and space vector machine to control the IPMSM in all operating conditions. The number of 1 to 6 in SVPWM represents sector number. Each sector is staged at 60 degrees. The sector is used to determine the switching sequence, i.e., from sector 1, 2, 3, 4, 5 and 6 respectively. It was then followed by a MATLAB or Simulink model to simulate the performance. The attainment of a satisfying result in modelling and simulation for both transient and steady-state conditions led to the deployment of the proposed framework in a real controller. It was tested with a dynamometer to investigate its performance in real-life conditions. It was also installed in a utility vehicle and made to perform certain tasks such as climbing a certain degree of inclination to evaluate the low RPM–high torque requirements and other generic tasks conducted daily by an electric vehicle.

One of the most important aspects of designing and developing an IPMSM or electric motor is the current and efficiency maps. However, it was discovered that only a small portion of the maps have been incorporated into the development of motor controllers. The focus has only been on the maximum values of DC-link voltage, current to be handled, and sustainable speed for a motor, while the point-to-point operating values are rarely considered. Subsequently, it led to several problems faced by the motor in its application, such as the instability at a certain point of operation, inefficiency, and the inability of the motor and controller to deal with the nonlinearity of real-life conditions.

The current and efficiency maps of the IPMSM under investigation were obtained in the design phase by modelling and simulating the PMSM using the finite element method and complex mathematical formula, as shown in Figure 6.

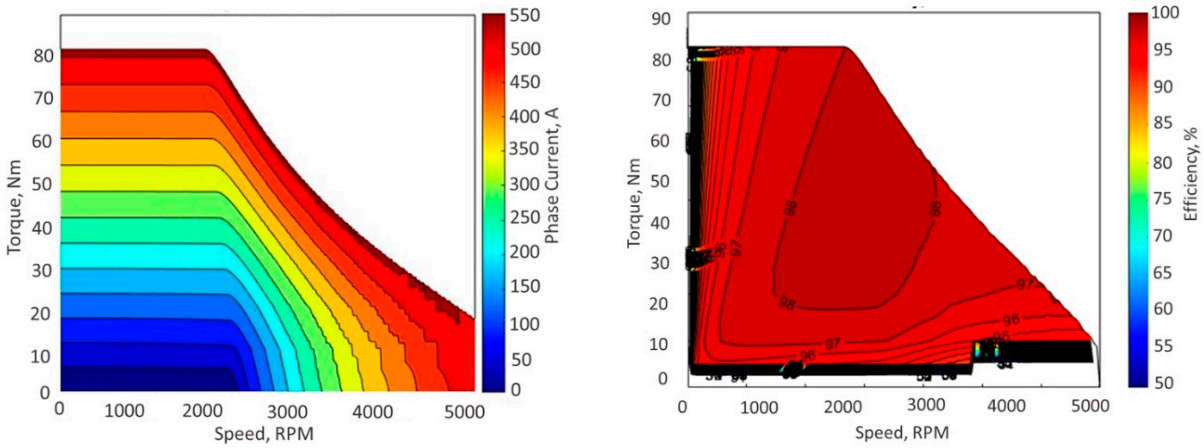

Figure 6. (**a**) Current requirement map of the IPMSM. (**b**) Efficiency maps of the IPMSM.

Figure 6a shows the current requirements at a specific speed (RPM) to produce torque (Nm), while Figure 6b indicates the IPMSM efficiency at any point or any given speed (RPM) and torque (Nm). The combination of the two maps, at any given speed and torque, made it possible to extract the values of the current and efficiency, which were subsequently used as inputs for the field-oriented control to eliminate the difficulties associated with estimating the current input. These difficulties have been previously identified by [17]. Moreover, Equation (14) shows the generated electromagnetic torque in an IPMSM is a function of i_q and i_d and the torque to be generated by the IPMSM in a real-life control application denoted as T_e^* is called a torque demand. This T_e^* can subsequently be used to calculate the value of i_q and i_d reference denoted as i_q^* and i_d^*. Meanwhile, Equation (14) shows the calculation of i_q^* and i_d^* is time-consuming and requires a lot of computer effort, thereby leading to a delay in the controller's performance. Therefore, both i_q^* and i_d^* were calculated offline in this research using the proposed lookup table for all the operating speed ranges, including the constant torque and field weakening.

2.3. Constant Torque Region

The IPMSM is operated at maximum torque per ampere (MTPA) in the constant torque region [28]. Therefore, Equation (5) was recalled, and the relationship between phase angle and the unit current electromagnetic torque was established as follows:

$$f(\theta) = \frac{T_e}{i_s} = \frac{3}{2}P\left[\psi_m \sin\theta + \frac{1}{2}(L_d - L_q)i_s \sin 2\theta\right] \tag{11}$$

Moreover, i_s was considered constant, and the following conditions were met to obtain the maximum torque per unit ampere.

$\frac{\partial f(\theta)}{\partial \theta} = 0$, and hence from Equation (11) becomes:

$$(L_d - L_q)i_s \cos 2\theta + \psi_m \cos\theta = 0$$

$$(L_d - L_q)i_s \left(2\cos^2\theta - 1\right) + \psi_m \cos\theta = 0$$

Solving the above equation:

$$\cos\theta = \frac{-\psi_m + \sqrt{{\psi_m}^2 + 8(L_d - L_q)^2 {i_s}^2}}{4(L_d - L_q)i_s} \tag{12}$$

i_q and i_d were also considered a function of phase angle (θ) as indicated in Figure 3, and this led to the establishment of a relationship as follows

$$i_d = \frac{-\psi_m + \sqrt{{\psi_m}^2 + 4(L_d - L_q)^2 {i_q}^2}}{2(L_d - L_q)} \tag{13}$$

Substituting Equation (13) to obtain maximum generated electromagnetic torque as in Equation (5) will be:

$$T_e = \frac{3}{4}Pi_q\left[\psi_m + \sqrt{{\psi_m}^2 + 4(L_d - L_q)^2 {i_q}^2}\right] \tag{14}$$

For the three-phase IPMSM, it can be deduced that $\psi_m = \sqrt{3}\psi_m$, $\psi_m = E_0/\omega_m$, where E_0 is the RMS of no-load back-EMF.

Equation (14) shows the governing equation for torque generated is only a function of i_q and this has to be maximum to maximize the torque. According to the phase angle representation of the current i_q and i_d , it is safe to set ${i_d}^* = 0$, while ${i_q}^*$ was obtained from the lookup table as previously explained.

2.4. Constant Power/Flux Weakening Region

The rotational speed of the IPMSM is over the base speed in the constant power/flux weakening region. The d-axis and the q-axis output voltage are limited by the maximum voltage on its DC-link bus voltage. Therefore, Equations (8)–(10) were applied to limit both the current and voltage of the IPMSM. These conditions led to the representation of Equation (10) as follows:

$$\left(\frac{r_s i_q}{\omega_r} + L_d i_d + \psi_m\right)^2 + \left(\frac{r_s i_d}{\omega_r} - L_q i_q\right)^2 \leq \frac{{v_{s_{Max}}}^2}{{\omega_r}^2} \tag{15}$$

Equation (15) stated that the IPMSM rotational speed is proportional to its stator voltage beyond its rated rotational speed. It means the values of i_q and i_d need to be adjusted to increase the rotational speed of the IPMSM while maintaining constant voltage in the stator. This process is called the IPMSM flux-weakening mechanism, which is possible by increasing the direct-axis demagnetization current. Flux-weakening control is a subject

of interest to several researchers [17,28–32], and their findings all agree the concept presents a serious challenge due to the involvement of the nonlinearity phenomenon. However, no exact solutions were found to deal with this problem, but they all agreed that it could be controlled by identifying $i_d{}^*$ and one technique commonly used in achieving this is the lookup table. This is due to the fact that it is difficult to accurately calculate several variables and parameters in the IPMSM in these nonlinear conditions.

This research used a one-dimensional lookup table based on speed feedback from the IPMSM to adjust the $i_d{}^*$ value. This is evident in the reduction of the torque generated in Equations (3)–(5) when the $i_d{}^*$ was set using negative values. Therefore, optimization is needed to limit the torque reduction, and an advanced angle θ was proposed by [29] as the optimization parameter. Meanwhile, Ref. [16] further elaborated that the phase angle should never exceed 450 or $\frac{\pi}{4}$ while [33,34] defined the $i_d{}^*$ in the flux-weakening region as follows.

$$i_d{}^* = \frac{\left(\frac{v_q}{\omega_r} - \psi_m\right)}{L_d} \tag{16}$$

or

$$i_d{}^* = \frac{-\psi_m}{L_d} \tag{17}$$

The value of the $i_q{}^*$ in the field-weakening region was derived by inserting Equation (16) into Equation (8). Therefore,

$$i_q{}^* = \sqrt{{i_{s_{Max}}}^2 - {i_d}^2} \tag{18}$$

2.5. Lookup Table Development

Previous explanations and Figure 5 show the proposed torque lookup table consisting of accelerator percentage (0–100%) and the IPMSM rotational speed (ω_r) used as inputs. It was intuitively designed based on the knowledge of how an IPMSM is expected to be operated throughout its range. It is important to note that the IPMSM was designed to be used for the electric vehicle traction motor. The fundamental requirement is that it should be able to provide the required torque and operating speed for the electric vehicle. As a consequence, it led to the explanation of the operating region for the IPMSM as follows.

Figure 7 shows the load on the electric vehicle is divided into at least three areas, including heavy, medium, and light load areas. The heavy load area is characterized by a large torque requirement represented by a high opening accelerator percentage at a very low RPM of the motor. The medium area has medium torque requirements with low to high RPM of the motor and the light load has a torque requirement with a low to high RPM of the motor. The other features presented in Figure 6 include the dynamic movements of driver request, which focus on how fast the torque was delivered. This phenomenon is represented using the acceleration or dotted line such that a steeper line indicates higher acceleration demanded by the driver. It is, however, important to note that there is practically an unlimited number of acceleration lines and a combination of torques and rotation speeds available to be selected by drivers in real life, and all of them occur nonlinearly. This is why controlling of such a nonlinear phenomenon is an interesting subject to explore.

Meanwhile, conventional vehicles already have advanced technology for such nonlinear demands, as indicated by the advanced control system in the engine control unit (ECU). However, an electric vehicle is a new technology without any current, mature, robust control algorithms for such nonlinearities, leading to the many approaches proposed as reported in previous studies. It is also important to note that the ECU technology used what is called engine mapping to define the parameters to be used in their controller and also used it to create a lookup table to define the relationship between engine loads and engine RPM. Subsequently, the torque and RPM values obtained were fed forward to the proportional controller to make the engine handle nonlinearities. This algorithm has been proven in conventional vehicle control technology and is used in this research.

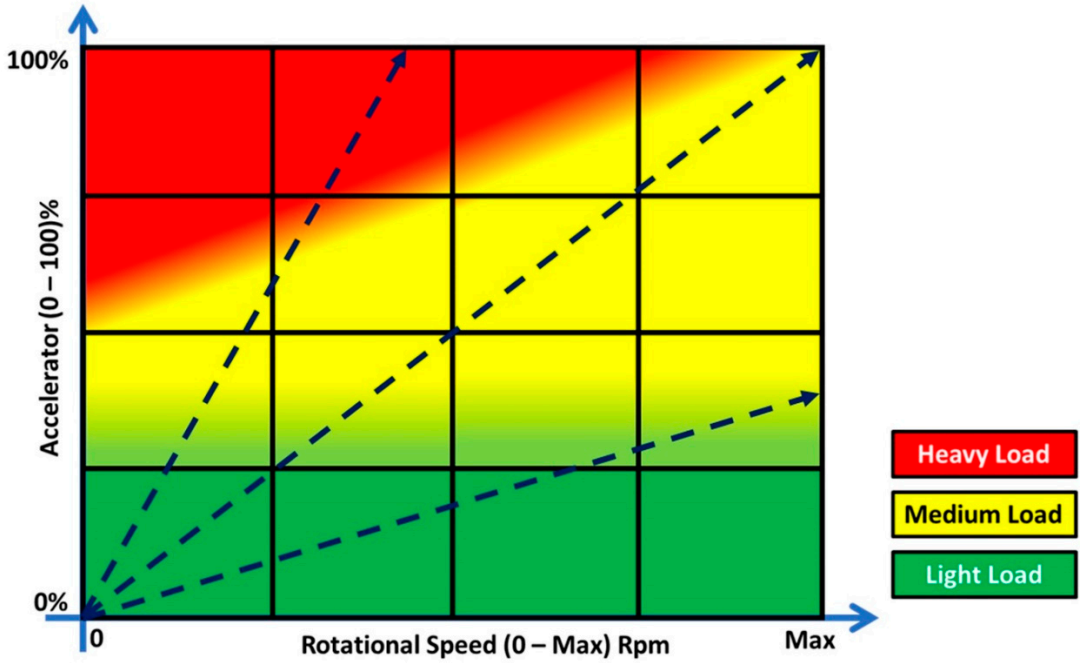

Figure 7. Load characteristics in an electric vehicle.

The lookup table for the IPMSM was also developed as observed in the ECU to provide torque generated by the IPMSM based on EV driver requests and the associated rotation speed. The proposed block diagram for the developed IPMSM controller is presented in Figure 8.

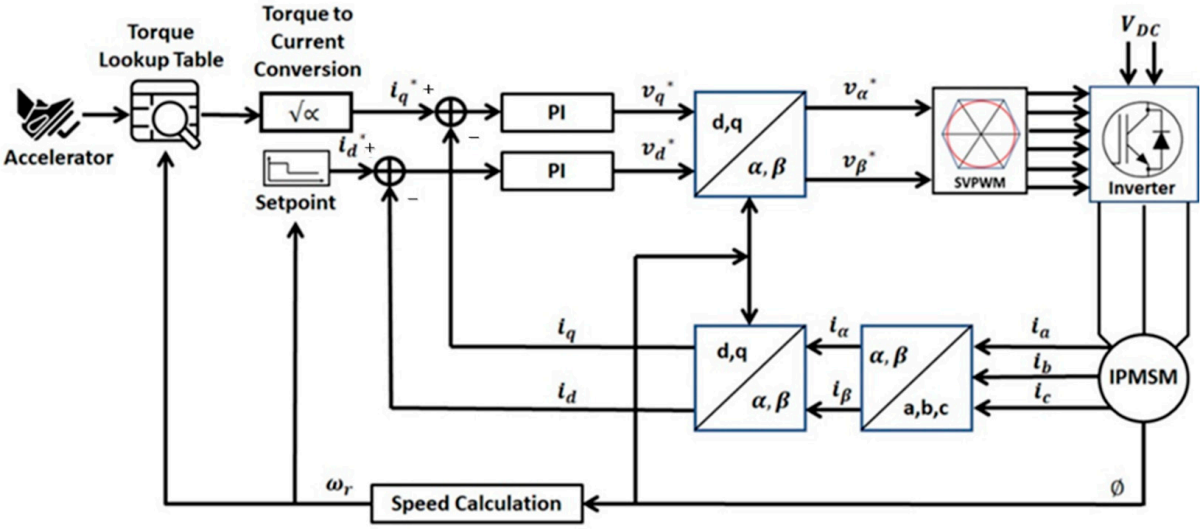

Figure 8. Proposed IPMSM lookup table-based controller block diagram.

Figure 8 shows the complete proposed IPMSM controller, which combines the lookup table to provide quadrature axis current denoted as $i_q{}^*$ and a setpoint function to provide direct axis current denoted as $i_d{}^*$. Both the lookup table and setpoint function were observed to have used the IPMSM rotational speed ω_r as their feedback input. The first lookup table to provide $i_q{}^*$ was designed, based on the explanation in Figures 6 and 7. Then it was used to create a 3D lookup table, as depicted in Figure 9.

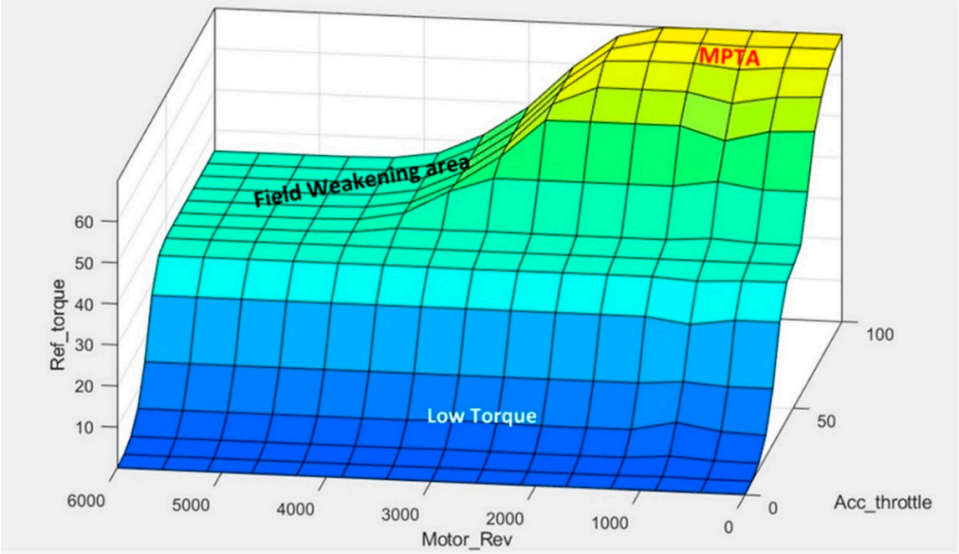

Figure 9. Three-dimensional lookup table for the IPMSM range of operation.

Figure 9 consists of three axes, including the Acc_Throttle, Motor_Ref, and Ref_Torque. The Acc_Throttle is the value from the accelerator movement of the electric vehicle, Motor_Rev is the IPMSM rotational speed, and Ref_Torque is the output of the lookup table, which was later converted into $i_q{}^*$. They were designed based on the three characteristics of the IPMSM load presented in Figure 7. It means the lookup table consists of a high load area defined as the MPTA in terms of the IPMSM torque generation, while the medium and light load areas were designed below the MPTA region. Meanwhile, light and medium loads with higher RPM requests or high-speed operation, flux-weakening area, and control were also considered.

The previous explanation shows that the lookup table was designed based on driver torque request. It was represented by how much the accelerator moved. This movement was subsequently fed to the lookup table consisting of the IPMSM mapping determined using FEM or dynamometer test. Moreover, the IPMSM MTPA dynamic equations explained were used to obtain the $i_q{}^*$ value which was eventually used as a function of rotational speed (ω_r, measured from the IPMSM) and inputted to the FOC-SVPWM control algorithm [35]. Another value set is the reference of direct axis current ($i_d{}^*$) which was defined to satisfy the constraint in Equation (15) and calculated in the field-weakening area where the target rotational speed is higher than the IPMSM rated or base speed according to the phase angle of 450 ($\frac{\pi}{4}$ rad) using Equations (16)–(18).

Then, the two reference values of $i_q{}^*$ and $i_d{}^*$ were fed forward to the FOC control algorithm using the space vector pulse width modulation. However, the FOC control algorithm is not comprehensively explained in this research, but further information is available in [36]. As is shown in Figure 8, the of $i_q{}^*$ and $i_d{}^*$ values are used as the setpoint or the PI controller before being fed into the FOC algorithm. It is important also to note that PI values both for of $i_q{}^*$ and $i_d{}^*$ inputs need to be defined.

The value of Kp (proportional gain) and Ki (integral gain) for the PI controller is tabulated in Table 2. These gains were suggested by the original Matlab/Simulink model from the Mathworks website [37].

Table 2. The value of Kp and Ki in PI controller.

	Kp	**Ki**
$i_q{}^*$	1.0744	1061.5
$i_d{}^*$	0.8779	710.3004

Subsequently, a complete model of the MATLAB/Simulink was developed to investigate the performance of the proposed lookup table algorithm integrated into the FOC-SVPWM, as indicated in Figure 8. The focus was on its ability to handle torque and speed requirements in normal operation, which is below MTPA, area of MTPA, and area of field weakening. The inputs used are presented in Figure 10, and these include accelerator movement (0–100%) and rotational speed of the IPMSM.

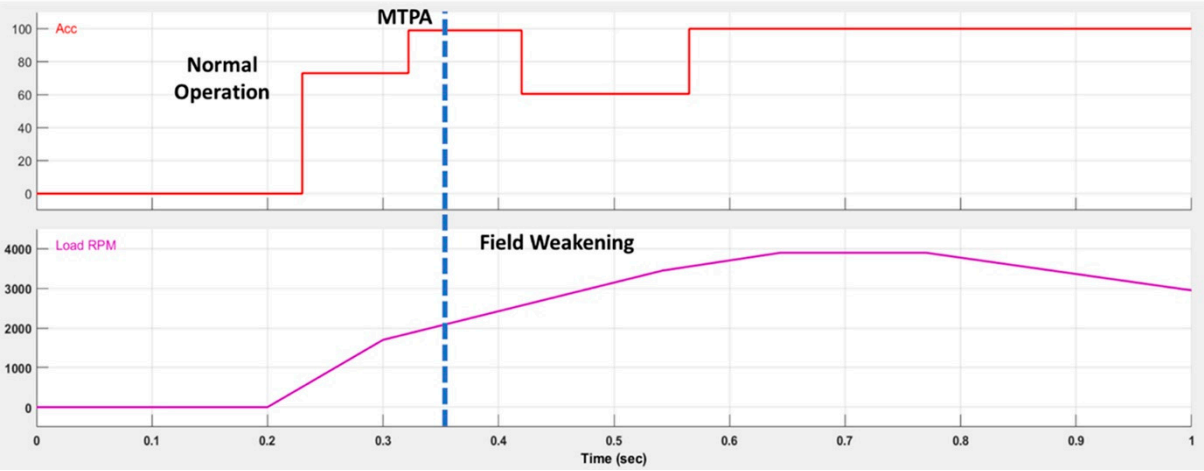

Figure 10. Controller simulation inputs.

The IPMSM is believed to be in normal operating conditions (from low torque to high torque, as indicated in Figure 9) when the rotational speed is less than 2000 RPM. Moreover, the motor is required to produce maximum torque when the accelerator reaches 100%, identified as the MTPA region. Meanwhile, the motor is expected to be operated in the field-weakening area when the rotational speed exceeds 2000 RPM. It is important to note that the torque generated in the field-weakening area is governed by the estimated torque set up in the lookup table. Therefore, the simulation results conform with the hypothesis as indicated in Figures 11–13.

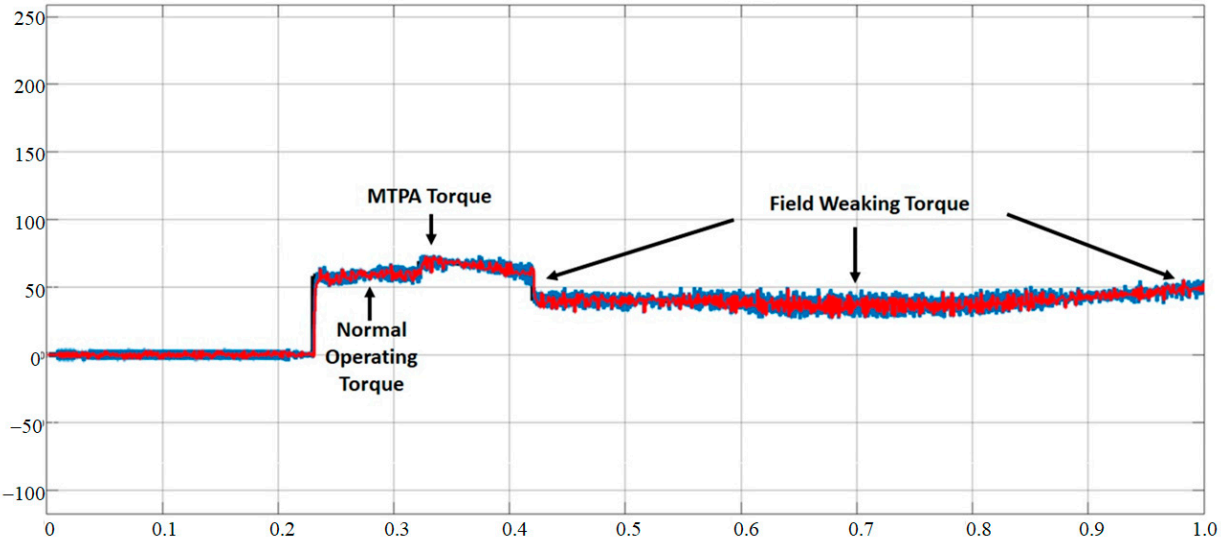

Figure 11. Torque output of the IPMSM using the proposed lookup table-based controller.

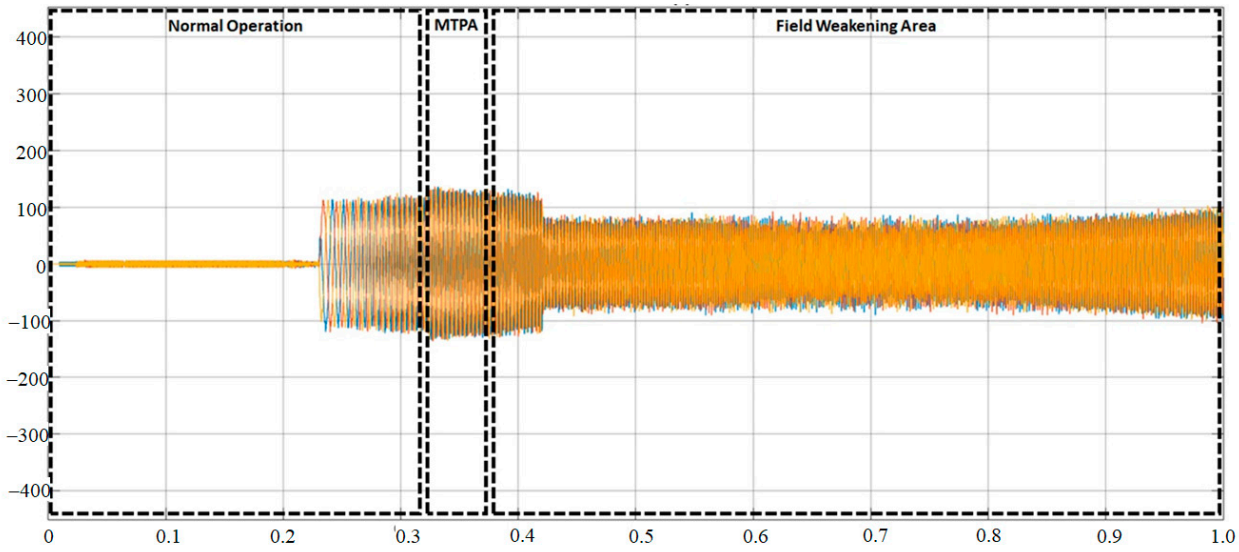

Figure 12. i_{abc} of the proposed controller.

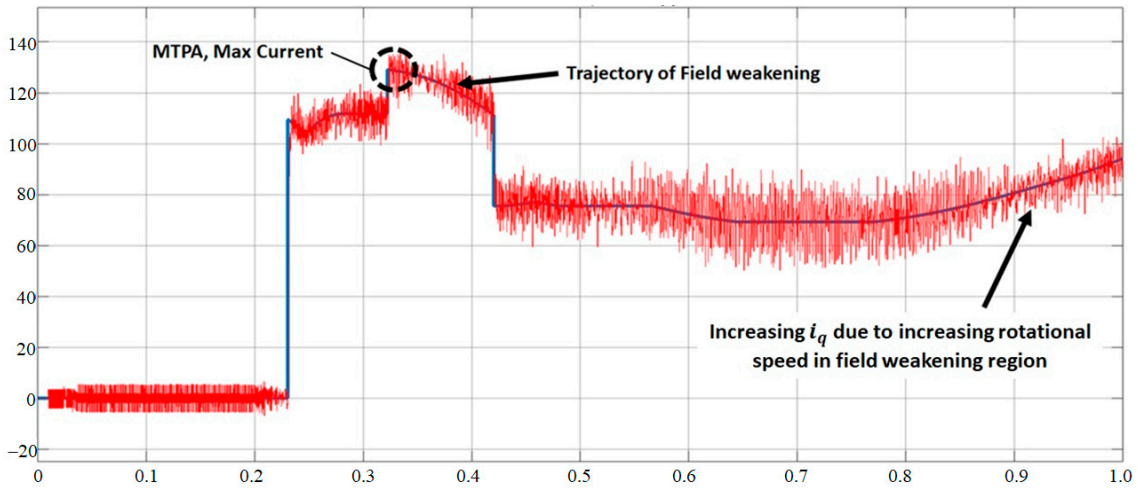

(**a**)

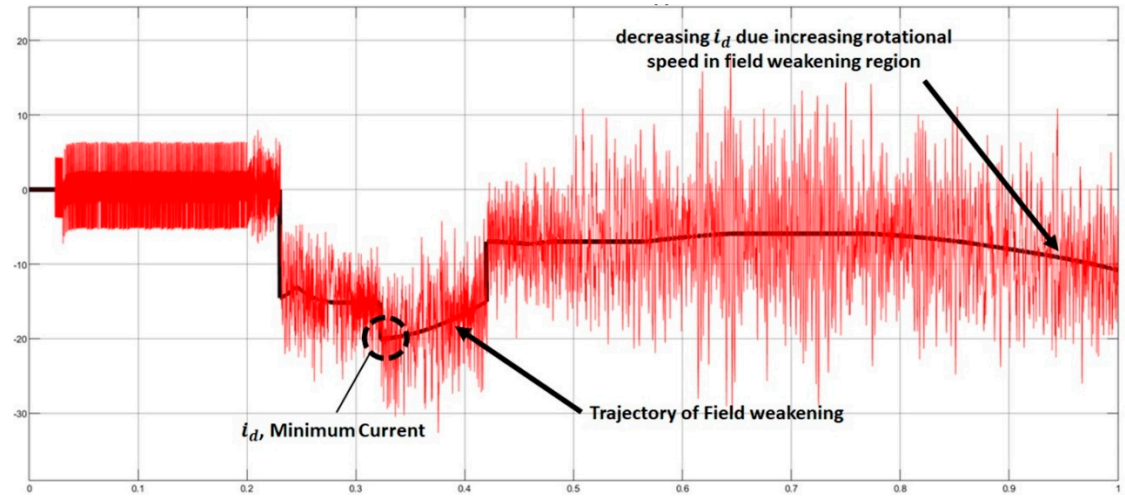

(**b**)

Figure 13. i_q (**a**) and i_d (**b**) current response from the simulation.

The torque output of the IPMSM controlled by the proposed lookup table controller is presented in Figure 11. The torque generated was observed to successfully match with the input requests in the whole operating torque and rotational speed range.

The controller was able to govern the IPMSM torque and rotational speed in the normal-operating, MTPA, and field-weakening regions. It was observed in the 60 Nm torque provided in the normal-operating region based on the request by 70% of the accelerator at a rotational speed below 2000 RPM. Maximum torque of 82 Nm, as specified in the specification in Table 1, was generated in the MTPA region with the accelerator depressed to 100% and the rotational speed recorded to be 2000 RPM. Meanwhile, in the field-weakening region where the rotational speed was more than 2000 RPM, the torque generated was reduced to 45 Nm, and this value was constant up to 4000 RPM, after which it reduced further to 40 Nm. The last part of Figure 11 shows the rotational speed was reduced below 4000 RPM. The torque generated is expected to be increased to reflect the constant power phenomenon according to the equation in the field-weakening region. It is what the controller and the IPMSM precisely did, as indicated in Figures 12 and 13.

Figure 12 shows the i_{abc} current profile of the controller. A distinct feature was observed in terms of the frequency and amplitude of the i_{abc} current sent to the IPMSM. The highest values for these parameters were observed in the MTPA region. At this region, the torque generated reached its maximum value. In the normal operation region, the torque generated is lower compared to torque in the MTPA region. In the field-weakening region, the torque value is the at its lowest value. It is reflecting the reduced torque due to field-weakening effects.

The phenomenon of the i_{abc} current was confirmed by the i_q and i_d evolution as indicated in Figure 13a,b, respectively. Equations (13) and (18) show the IPMSM can be operated in the MTPA region where its rotational speed is less than its base speed and the i_q value was observed to range from zero up to a maximum of 145 A, while the i_d was from zero up to a minimum of -20 A in the region. Meanwhile, the values of these parameters were set according to the constant power equation in the field-weakening area. The i_q was observed to reduce when the rotational speed increased while the i_d showed a contrasting result.

The simulation results showed the controller effectively handled all the requests for torque delivery at each operating and rotational speed range, including the field-weakening area. Therefore, the next step was to develop the controller to control the IPMSM motor in real life with a dynamometer used to evaluate its performance in this condition.

3. Experimental Set-Up of the Proposed PMSM Controller

The controller was developed based on the modeling and simulation results previously explained with the modular concept built to have three separate modules: the main controller, the controller driver, and the MOSFET circuit. It was produced to have the ability to handle 15 kW rated power with a peak of 30 kW. The DC-link bus was designed to be 125 V with a nominal voltage of 100 V. This means the controller is capable of handling phase current up to 300 A. The snapshots of the designed and developed controller are, therefore, presented in Figure 14.

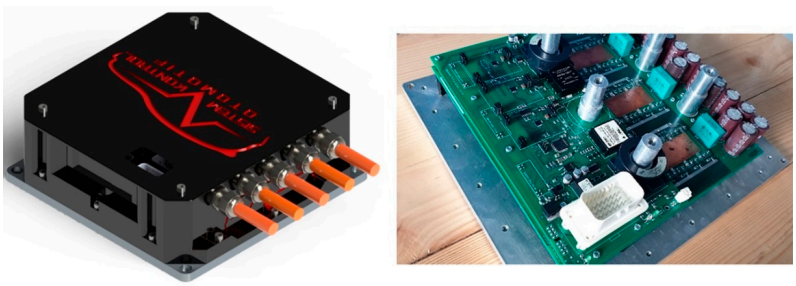

Figure 14. Snapshot of the developed controller.

The controller software was also developed to incorporate the proposed lookup table into the field-oriented control and space vector machine algorithm with the interface indicated in Figure 15. Figure 15 shows that the lookup table consists of three axes: the TPS (torque position sensor—which measures the percentage movement of the accelerator), the rotational speed of the motor/RPM, and torque setting. The user interface can, therefore, be easily used by a user to program the value of each torque as a function of % TPS and RPM.

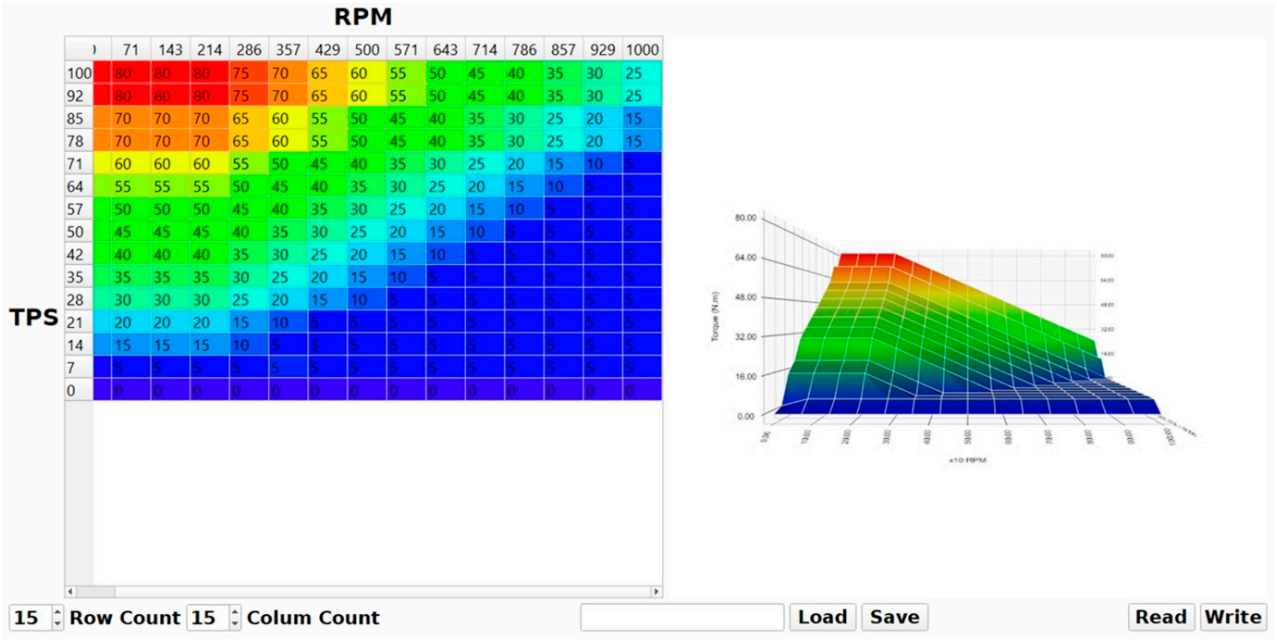

Figure 15. Snapshot of the lookup table interface of the controller software.

Some experimental activities were also conducted to investigate the newly designed controller and the IPMSM in real-life conditions using a dynamometer. The set-up of the experiment is indicated in the following Figure 16. The snapshot of the testing process is also presented in Figure 17. Figure 16 shows the possibility of preprogramming the load of the eddy current dynamometer used in the experiment using computer control.

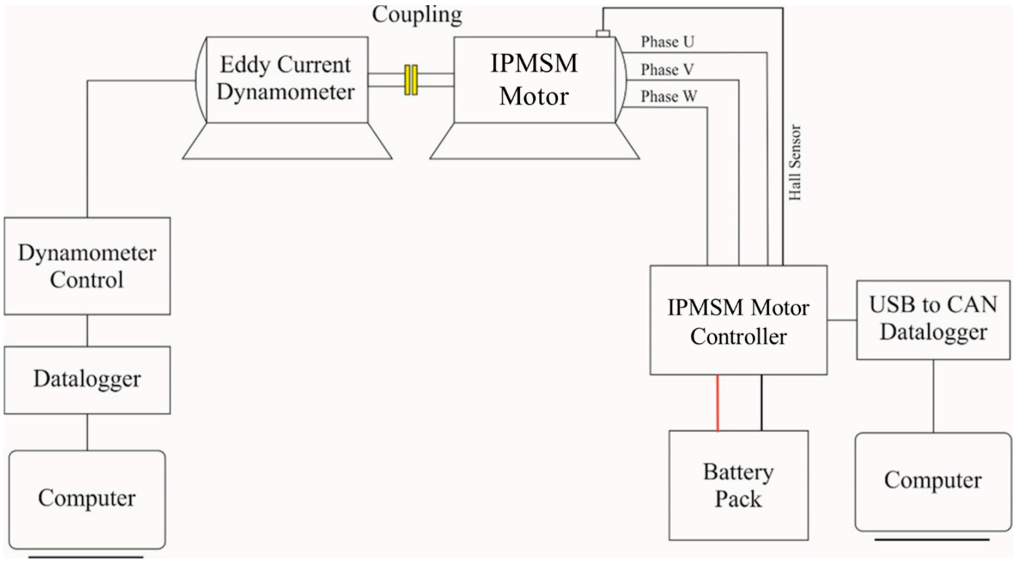

Figure 16. Experimental set-up of IPMSM and its controller performance measurement.

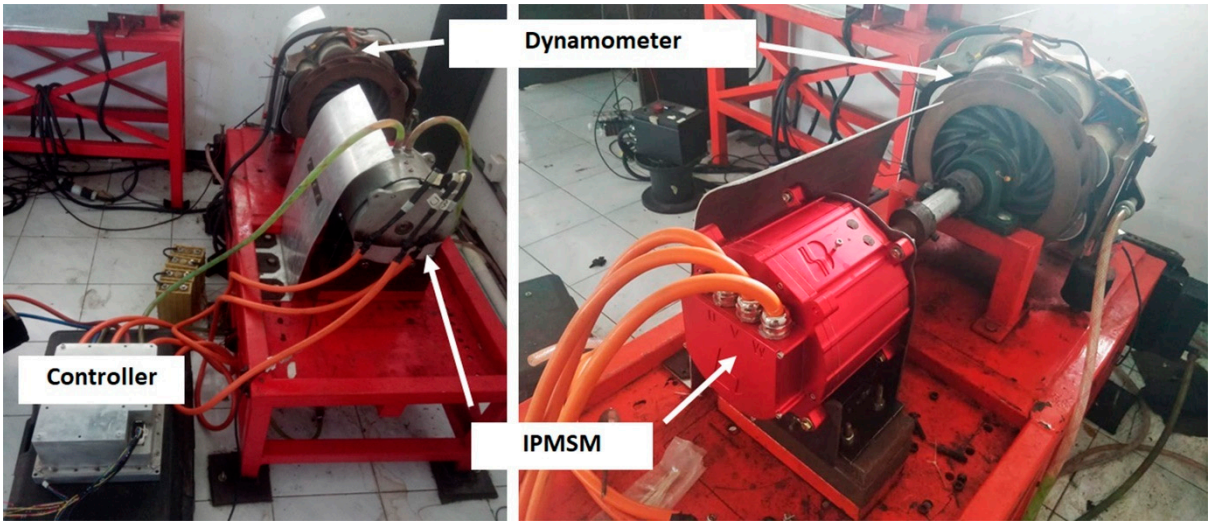

Figure 17. Snapshot of the experimental set-up of IPMSM and its controller performance measurement.

The dynamometer software recorded all the necessary graphs, including the torque vs. speed and power vs. speed. The results presented in Figure 18 showed the controller controlled the IPMSM throughout its whole operating condition, including the MTPA and the field-weakening regions. Meanwhile, the MPTA region was determined by the constant torque with the IPMSM discovered to have produced 77 Nm from zero to 1500 RPM and the value reduced to 10 Nm beyond 1500 RPM and up to 5500 RPM was the field-weakening region.

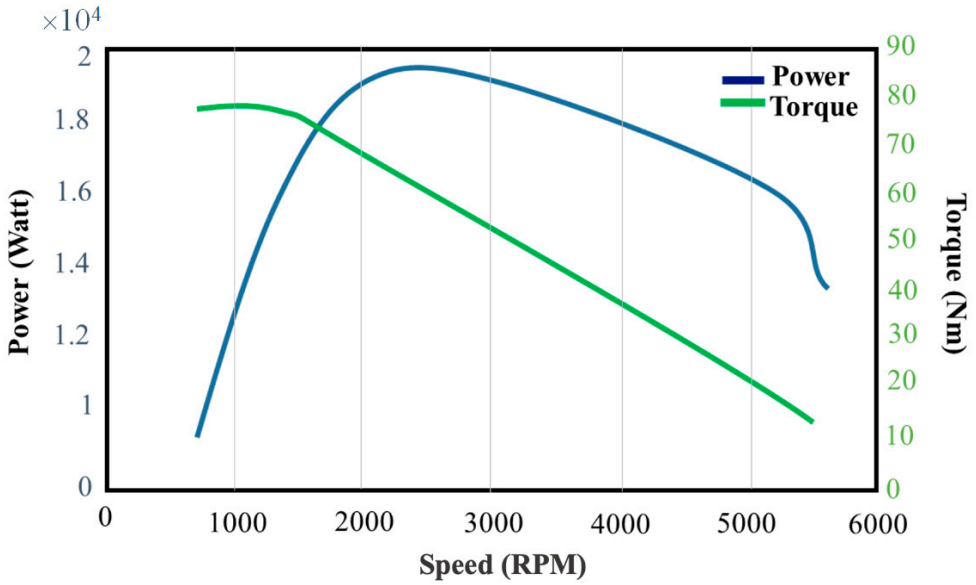

Figure 18. The experimental test results of the IPMSM and its controller using an eddy current dynamometer.

4. Discussions and Analysis

Experimental tests were conducted to determine the performance of the proposed lookup table-based controller in real-life conditions, and the results are presented in the form of a torque versus RPM graph in Figure 18. This graph was also compared with the graphs generated to show its design phase performance from the simulation conducted using FEM, as indicated in Figure 19.

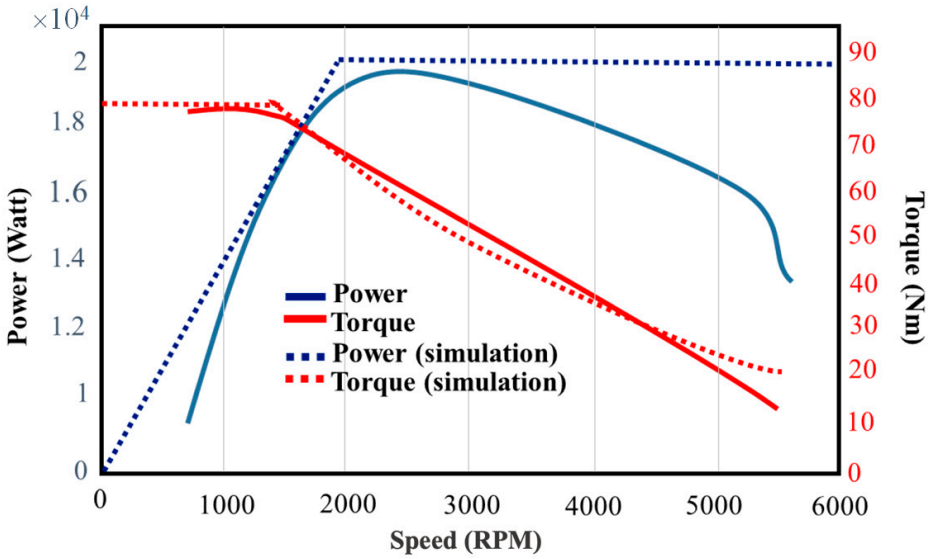

Figure 19. Performance comparison between the FEM simulation and experimental test results of the IPMSM and the proposed controller.

Figure 19 shows the proposed lookup table-based controller successfully controlled the IPMSM in real-life operating conditions. It was indicated by the better torque generated at the MTPA region than in the simulation design due to the absence of the effect of the mechanical dynamics at the initial starting speed of the IPMSM. Moreover, the maximum torque generated in the test was 80 Nm, while only 75 Nm was produced in the simulation, indicating a 7% increase.

The base speed of the IPMSM in the experimental test was found to be 25% lower before the torque decreased, as indicated by the 2000 RPM in simulation and only 1500 RPM during the experiment. This phenomenon was associated with the effect of the mechanical dynamics on IPMSM performance at higher RPM. For example, friction is a function of rotational speed such that a higher rotation causes more friction. This effect was evident in the field-weakening or constant power region, with the power and maximum speed found to be lower during the experimental test than the simulation. The real power was recorded to be only 19 kW in the experimental result compared to 20 kW in simulation, which is only a 5% reduction, while maximum speed was 5500 RPM and 6000 RPM, respectively. This indicates an 8% reduction. Therefore, the full results of the comparison are presented in the following Table 3.

Table 3. Performance comparison of the IPMSM and its proposed lookup table-based controller.

	Constant Torque Region		Field-Weakening Region	
	Torque (Nm)	**Base Speed (RPM)**	**Power (kW)**	**Max. Speed (RPM)**
Simulation	75	2000	20	6000
Experimental	80	1500	19	5500
Difference	7%	−25%	−5%	−8%

Further analysis in the field-weakening region showed that the experimental torque generated was smaller than in simulation. The result is as expected. The higher the speed of the motor, the smaller the torque generated. In terms of power generated, in the high speed region, the power was also reduced. This is due to the friction occurring in the IPMSM. With the increasing rotational speed, the friction became greater. The phenomena occurring in the high rotational speed is not a problem. In the region, the vehicle tends to need more rotational speed instead of torque and power. It reflects the load requirements as presented in Figure 7. In the region, the load requirements are low, hence low torque

and power are required. In terms of practical implementation, constant power at high rotational speed is not required. Usually at this point, the vehicle will only need smaller torque to maintain/increase speed. However, if it should require larger torque then the proper design of a gearbox ratio is required.

The proposed controller in this paper was implemented in an off-road vehicle [21]. It has a two speed gearbox with ratios of 1:32 and 1:16. It is depicted in Figure 20 as the following.

Figure 20. Off-road vehicle as the controller platform implementation.

Regarding performance comparisons with other known models of controller algorithms as described in [19,20], the proposed controller reported in this paper was similar in performance. The proposed controller successfully met its intended target, which was regulating the IPMSM performance in the MTPA and the field-weakening region. It was also the case with [19,20].

5. Conclusions

The comparison of the real-life conditions and simulation performance shows the proposed 3D lookup table-based controller worked effectively in all the operating ranges. It can efficiently control the IPMSM at a constant torque or the maximum torque per ampere region to produce a slightly higher maximum torque than during the simulation phase. Meanwhile, it had lower performance in the constant power region than the simulation due to the contribution of the mechanical dynamics of friction and other losses. The effect of the friction, which is a nonlinear phenomenon, was observed to be more obvious in the higher RPM region due to the increase in the RPM, thereby reducing the motor power of the experimental test compared to the simulation. It is important to note that it is impossible to model this nonlinear phenomenon properly in the MATLAB/Simulink model.

This analysis showed that the proposed controller was effective and efficient, as indicated by its ability to control the motor to produce torque higher than 7% in the constant torque region and reach a rotational speed of 5500 RPM compared to the simulated 6500 RPM in the field-weakening region. It will, therefore, be interesting to assess its ability to handle daily requirements when installed in an electric vehicle, and this is recommended for further study. Another proposed further study was to reduce the chattering phenomenon observed in Figure 13. One proposed solution is to employ a fuzzy logic engine in the controller algorithm. It will be interesting to see the performance of such an intelligent controller to cope with the nonlinearity phenomenon that occurred in the IPMSM.

Author Contributions: Conceptualization, M.N.Y.; methodology, M.N.Y.; software, M.N.Y. and Y.U.N.; validation, M.N.Y., I.S. and Y.Y.; formal analysis, M.N.Y.; investigation, M.N.Y.; resources, M.N.Y., Y.U.N. and I.S.; data curation, M.N.Y.; writing—original draft preparation, M.N.Y.; writing—review and editing, M.N.Y., I.S. and Y.Y.; visualization, I.S., Y.Y. and Y.U.N.; supervision, M.N.Y.; project administration, M.N.Y. and I.S.; funding acquisition, M.N.Y. All authors have read and agreed to the published version of the manuscript.

Funding: This research was funded by the Lembaga Pengelola Dana Pendidikan (LPDP) with contract number PRJ-5/LPDP/2020.

Institutional Review Board Statement: Not applicable.

Informed Consent Statement: Not applicable.

Data Availability Statement: Not applicable.

Conflicts of Interest: The authors declare no conflict of interest.

References

1. Benchaib, A.; Poullain, S.; Thomas, J.L.; Alacoque, J.C. Discrete-Time Field-Oriented Control for SM-PMSM Including Voltage and Current Constraints. In Proceedings of the IEEE International Electric Machines and Drives Conference, IEMDC'03, Madison, WI, USA, 1–4 June 2003; Volume 4. [CrossRef]
2. Feng, C.; Chaoying, X.; Xiaoxin, H. Study on the Losing Control Problem of Direct Torque Control in Permanent Magnet Synchronous Motor Drive. *Trans. Inst. Meas. Control* **2018**, *41*, 504–515. [CrossRef]
3. Kommula, B.N.; Kota, V.R. Journal of King Saud University–Engineering Sciences Direct Instantaneous Torque Control of Brushless DC Motor Using Firefly Algorithm Based Fractional Order PID Controller. *J. King Saud Univ.-Eng. Sci.* **2018**, *32*, 133–140. [CrossRef]
4. Vajsz, T.; Számel, L.; Rácz, G. A Novel Modified DTC-SVM Method with Better Overload-Capability for Permanent Magnet Synchronous Motor Servo Drives. *Period. Polytech. Electr. Eng. Comput. Sci.* **2017**, *61*, 253–263. [CrossRef]
5. Zurbriggen, F.; Ott, T.; Onder, C.H. Fast and Robust Adaptation of Lookup Tables in Internal Combustion Engines: Feedback and Feedforward Controllers Designed Independently. *Proc. Inst. Mech. Eng. Part D J. Automob. Eng.* **2015**, *230*, 723–735. [CrossRef]
6. Benfriha, E.; Mansouri, A.; Bendiabdellah, A.; Boufadene, M. Engineering Sciences Nonlinear Adaptive Observer for Sensorless Passive Control of Permanent Magnet Synchronous Motor. *J. King Saud Univ.-Eng. Sci.* **2019**, *32*, 510–517. [CrossRef]
7. Carpiuc, S.C.; Lazar, C. Fast Real–Time Constrained Predictive Current Control in Permanent Magnet Synchronous Machine Based Automotive Traction Drives. *IEEE Trans. Transp. Electrif.* **2015**, *1*, 326–335. [CrossRef]
8. Pollex, V.; Feld, T.; Slomka, F.; Margull, U.; Mader, R.; Wirrer, G. Sufficient Real-Time Analysis for an Engine Control Unit with Constant Angular Velocities. In Proceedings of the 2013 Design, Automation & Test in Europe Conference & Exhibition (DATE), Grenoble, France, 18–22 March 2013; pp. 5–8. [CrossRef]
9. Liang, P.; Pei, Y.; Chai, F.; Zhao, K. Analytical Calculation of D-and Q -Axis Inductance. *Energies* **2016**, *9*, 580. [CrossRef]
10. Chen, Z. Maximum Torque Per Ampere and Flux-Weakening Control for PMSM Based on Curve Fitting. In Proceedings of the 2010 IEEE Vehicle Power and Propulsion Conference, Lille, France, 3 September 2010; Volume 4, pp. 3–7. [CrossRef]
11. Jahns, T.M. Flux-Weakening Regime Operation of an Interior Permanent-Magnet Synchronous Motor Drive. *IEEE Trans. Ind. Appl.* **1987**, *IA-23*, 681–689. [CrossRef]
12. Sudhoff, S.; Corzine, K.; Hegner, H. A Flux Weakening Strategy for Current Regulated Surface Mounted Permanent Magnet Machine Drives. *IEEE Trans. Energy Convers.* **1995**, *10*, 431–437. [CrossRef]
13. Kwon, Y.; Kim, S.; Sul, S. Voltage Feedback Current Control Scheme for Improved Transient Performance of Permanent Magnet Synchronous Machine Drives. *IEEE Trans. Ind. Electron.* **2012**, *59*, 3373–3382. [CrossRef]
14. Lin, P.; Lai, Y. Voltage Control Technique for the Extension of DC-Link Voltage Utilization of Finite-Speed SPMSM Drives. *IEEE Trans. Ind. Electron.* **2012**, *59*, 3392–3402. [CrossRef]
15. Balashanmugham, A.; Maheswaran, M. Permanent-Magnet Synchronous Machine Drives. 2019. Available online: https://www.intechopen.com/chapters/68961 (accessed on 20 May 2022).
16. Luo, G.; Zhang, R.; Chen, Z.; Tu, W.; Zhang, S.; Kennel, R.; Member, S. A Novel Nonlinear Modeling Method for Permanent Magnet Synchronous Motors. *IEEE Trans. Ind. Electron.* **2016**, *46*, 6490–6498. [CrossRef]
17. Nanfang, Y.; Guangzhao, L.U.O.; Weiguo, L.I.U.; Kang, W. Interior Permanent Magnet Synchronous Motor Control for Electric Vehicle Using Look-up Table. In Proceedings of the 7th International Power Electronics and Motion Control Conference, Harbin, China, 2–5 June 2012; Volume 3, pp. 1015–1019. [CrossRef]
18. Hu, D.; Xu, L. Characterizing the Torque Lookup Table of an IPM Machine for Automotive Application. In Proceedings of the 2014 IEEE Conference and Expo Transportation Electrification Asia-Pacific (ITEC Asia-Pacific), Beijing, China, 31 August–3 September 2014. [CrossRef]
19. Ji, Y.B.; Lee, J.H. Feedforward Interpolation Error Compensation Method for Field Weakening Operation Region of PMSM Drive. *Electronics* **2019**, *8*, 1052. [CrossRef]

20. Kim, D.Y.; Lee, J.H. Compensation of Interpolation Error for Look-up Table-Based Pmsm Control Method in Maximum Power Control. *Energies* **2021**, *14*, 5526. [CrossRef]
21. Yuniarto, M.N.; Nugraha, Y.U.; Negara, I.M.Y.; Asfani, D.A.; Sidharta, I. Designing and Performance Investigation of Permanent Magnet Motor Prototype for UTV Electric Drive Train Application. *Int. J. Power Electron. Drive Syst.* **2021**, *12*, 2018–2029. [CrossRef]
22. Thike, R.; Member, S.; Pillay, P. Mathematical Model of an Interior PMSM with Aligned Magnet and Reluctance Torques. *IEEE Trans. Transp. Electrif.* **2020**, *6*, 647–658. [CrossRef]
23. Barcaro, M.; Bianchi, N. Interior PM Machines Using Ferrite to Substitute Rare–Earth Surface PM Machines. In Proceedings of the 2012 XXth International Conference on Electrical Machines, Marseille, France, 2–5 September 2012; pp. 1339–1345. [CrossRef]
24. Bilgin, B.; Member, S.; Liang, J.; Terzic, M.V.; Dong, J.; Member, S.; Trickett, E.; Emadi, A. Modeling and Analysis of Electric Motors: State-of-the-Art Review. *IEEE Trans. Transp. Electrif.* **2019**, *5*, 602–617. [CrossRef]
25. Lee, H. Characteristic Analysis of a V-Shape Interior Permanent Magnet Synchronous Motor According to Design Parameter. In Proceedings of the 2018 21st International Conference on Electrical Machines and Systems (ICEMS), Jeju, Korea, 7–10 October 2018; pp. 505–509. [CrossRef]
26. Qi, G.; Chen, J.T.; Zhu, Z.Q.; Howe, D.; Zhou, L.B.; Gu, C.L. Influence of Skew and Cross-Coupling on Flux-Weakening Performance of Permanent-Magnet Brushless AC Machines. *IEEE Trans. Magn.* **2009**, *45*, 2110–2117. [CrossRef]
27. Vagati, A.; Boazzo, B.; Guglielmi, P. Design of Ferrite-Assisted Synchronous Reluctance Machines Robust Toward Demagnetization. *IEEE Trans. Ind. Appl.* **2014**, *50*, 1768–1779. [CrossRef]
28. Zhang, H.; Dou, M.; Deng, J. Loss-Minimization Strategy of Non-Sinusoidal Back-EMF PMSM in Multiple Synchronous Reference Frames. *IEEE Trans. Power Electron.* **2019**, *35*, 8335–8346. [CrossRef]
29. Deng, T.; Su, Z.; Li, J.; Tang, P.; Chen, X.; Liu, P. Advanced Angle Field Weakening Control Strategy of Permanent Magnet Synchronous Motor. *IEEE Trans. Veh. Technol.* **2019**, *9545*, 3424–3435. [CrossRef]
30. Pan, C.; Sue, S. A Linear Maximum Torque Per Ampere Control for IPMSM Drives Over Full-Speed Range. *IEEE Trans. Energy Convers.* **2005**, *20*, 359–366. [CrossRef]
31. Wang, J.; Jing, M.; Fan, H.; Liu, H.; Shi, B. Study on Unbalance Magnetic Pull of the Motorized Spindle under Different Rotor Eccentricities. In Proceedings of the 13th International Conference on Ubiquitous Robots and Ambient Intelligence (URAl), Xi'an, China, 19–22 August 2016; pp. 781–785. [CrossRef]
32. Zhang, K.; Li, G.J.; Zhu, Z.Q.; Jewell, G.W. Investigation on Contribution of Inductance Harmonics to Torque Production in Multiphase Doubly Salient Synchronous Reluctance Machines. *IEEE Trans. Magn.* **2019**, *55*, 1–10. [CrossRef]
33. Fadel, M.; Sepulchre, L.; David, M.; Porte, G. MTPV Flux Weakening Strategy for PMSM. *IEEE Trans. Ind. Appl.* **2018**, *54*, 6081–6089. [CrossRef]
34. Miguel-espinar, C.; Heredero-peris, D.; Gross, G.; Llonch-masachs, M.; Montesinos-miracle, D.; Member, F. Maximum Torque per Voltage Flux-Weakening Strategy with Speed Limiter for PMSM Drives. *IEEE Trans. Ind. Electron.* **2020**, *68*, 9254–9264. [CrossRef]
35. Inoue, T.; Inoue, Y.; Morimoto, S.; Sanada, M. Mathematical Model for MTPA Control of Permanent-Magnet Synchronous Motor in Stator Flux Linkage Synchronous Frame. *IEEE Trans. Ind. Appl.* **2015**, *9994*, 3620–3628. [CrossRef]
36. Bose, B.K. *Power Electronics and Variable Frequency Drives*, 1st ed.; Knoville, Ed.; IEEE Press: New York, NY, USA, 1997.
37. PMSM Field-Weakening Control. Available online: https://www.mathworks.com/help/physmod/sps/ug/pmsm-field-weakening-control.html#d123e41959 (accessed on 13 May 2022).